

The numerical simulation of interacting galaxies by means of hybrid supercomputers*

I. Kulikov, I. Chernykh, E. Katysheva, V. Protasov, A. Serenko

Abstract. In this paper, a new hydrodynamic numerical simulation of interacting galaxies is proposed. The main subgrid physics processes are: the star formation, the supernovae feedback, the cooling function and the molecular hydrogen formation. The collisionless hydrodynamic approach was used for the simulation of the stars and dark matter. An approach for constructing a high order accurate numerical method for solving hydrodynamic equations is described. This method is based on a combination of the operator-splitting method, the Godunov method, and the piecewise-parabolic method on a local stencil. In addition, the performance of the numerical method is demonstrated on a global test of the central galaxies interaction.

1. Introduction

The movement of galaxies in dense clusters turns the collisions of galaxies to an important evolutionary factor, because during the Hubble time an ordinary galaxy may suffer up to ten collisions with the galaxies of its cluster [1]. In interacting galaxies, the subgrid physics problem: the star formation [2], the AGN, and the supernovae feedback [3], the formation of supermassive black holes [4, 5], chemistry [6], plays the key role. One of the most important fundamental processes, affecting the molecular clouds formation as well as the formation of the Universe, is the process of the molecular hydrogen evolution [7, 8].

One of the main problems of the galaxy simulation is the scale ratio. A typical galaxy can have the mass of 10^{13} Solar masses and the size of 10^4 parsecs, resulting in 13 order gap for the mass and 14 order gap for the size in comparison with the Sun. Therefore, in order to simulate complex astrophysical processes with a high resolution it is necessary to use the best available supercomputers. Two of the top three (five of the top ten) supercomputers listed in the 2014 November version of the Top 500 list fit graphic accelerators and Intel Xeon Phi accelerators. Most likely, the first ExaScale performance supercomputer will be built based on the hybrid approach. The code development for the hybrid supercomputers is not a solely technical problem, but an individual

*Supported by the Russian Foundation for Basic Research under Grants 15-31-20150 and 14-01-31199 and under Grant of the President of Russian Federation for the support of young scientists No. MK-6648.2015.9.

complex scientific problem, requiring co-design of algorithms at all stages of the solving problem: from the physical statement to the development tools.

During the last two decades, two main approaches were used for the numeral hydrodynamics simulations of astrophysical flows: the Lagrangian smooth particle hydrodynamics methods (hereafter, the SPH method) and Eulerian mesh-based methods. Numerous comparisons between the SPH and the mesh-based methods have been performed [9, 10]. The main disadvantages of most of the SPH methods are the inaccurate computation of large gradients and discontinuities [11], suppression of physical instabilities [9], the difficulties with choosing a proper smoothing kernel [12] and the use of artificial viscosity [13]. The main disadvantages of most of the mesh-based methods are their Galilean non-invariance on a mesh [10, 14], the difficulties with coding and implementation, and difficulties with treating multi-component systems, such as stars and gas [15, 16]. During the last decade, the combined Eulerian–Lagrangian approach was developed and actively used for numerical simulations of astrophysical hydrodynamics flows [17, 18]. These methods unite the advantages of both approaches, while attempting to reduce the disadvantages.

There are several well-known high-order numerical hydrodynamics methods such as the MUSCL (Monotonic Upstream-Centered Scheme for Conservation Laws) method [19, 20], the total variation diminishing (TVD) method [21], and the piecewise parabolic method (PPM) [22]. The general idea of their approaches is in constructing a piecewise-polynomial function on each cell of the numerical mesh. It may be a piecewise-linear reconstruction (in the case of the MUSCL scheme) or a piecewise-parabolic reconstruction (in the case of the PPM method). For constructing a monotonized numerical solution (needing to avoid the growth of spurious extrema), the limiters are usually employed in the TVD methods [23]. The problem of selecting limiters is analogous to the choice of artificial viscosity in SPH methods: a wrong choice of artificial viscosity for the SPH method (or limiters for the TVD method) can cause a considerable distortion of the numerical solution. The PPM method does not have the monotonicity problem, because piecewise-polynomial solutions on each cell are constructed without extrema. The main disadvantage of the PPM method is the use of a non-local stencil for computing the hydrodynamic quantities at the next time step. The non-local stencil has problems with a proper choice of boundary conditions, domain decomposition, and dissipation of the numerical solution. To resolve these problems, a modification of the PPM method was proposed: the so-called piecewise-parabolic method on a local stencil (PPML) [24, 25]. The main idea of the PPML method is the use of a piecewise parabolic numerical solution on the previous time step for computing the Riemann problem.

2. The numerical model of interacting galaxies

The numerical model of interacting galaxies is based on the solution of one-velocity gravitational gas dynamics equations describing the mixture of atomic and molecular hydrogen, the equation describing variations of molecular hydrogen density, and the "collisionless" hydrodynamic approach for the description of the stars and dark matter [16]. The numerical model by means subgrid physics processes: star formation, supernovae feedback, cooling function and molecular hydrogen formation, has been extended.

2.1. The gravitation hydrodynamic equations. We use the 3D model of self-gravitating gas dynamics in the Cartesian coordinate system, including an extended set of equations for the gas dynamics in a divergence form, closed by an equation of state for an ideal gas. A set of equations is supplemented by the Poisson equation for the potential of a gaseous component:

$$\begin{aligned}
\frac{\partial \rho}{\partial t} + \nabla \cdot (\rho \vec{u}) &= \mathcal{S} - \mathcal{D}, \\
\frac{\partial \rho_H}{\partial t} + \nabla \cdot (\rho_H \vec{u}) &= -s_{H,H_2} + \mathcal{S} \frac{\rho_H}{\rho} - \mathcal{D}^H \frac{\rho_H}{\rho}, \\
\frac{\partial \rho_{H_2}}{\partial t} + \nabla \cdot (\rho_{H_2} \vec{u}) &= s_{H,H_2} + \mathcal{S} \frac{\rho_{H_2}}{\rho} - \mathcal{D} \frac{\rho_{H_2}}{\rho}, \\
\frac{\partial \rho \vec{u}}{\partial t} + \nabla \cdot (\rho \vec{u} \vec{u}) &= -\nabla p - \rho \nabla(\Phi) + \vec{v} \mathcal{S} - \vec{u} \mathcal{D}, \\
\frac{\partial \rho E}{\partial t} + \nabla \cdot (\rho E \vec{u}) &= -\nabla \cdot (p \vec{v}) - (\rho \nabla(\Phi), \vec{u}) - \Lambda + \Gamma - \varepsilon \frac{\mathcal{D}}{\rho}, \\
\frac{\partial \rho \varepsilon}{\partial t} + \nabla \cdot (\rho \varepsilon \vec{u}) &= -(\gamma - 1) \rho \varepsilon \nabla \cdot \vec{u} - \Lambda + \Gamma - \varepsilon \frac{\mathcal{D}}{\rho}, \\
\rho E &= \frac{1}{2} \rho \vec{u}^2 + \rho \varepsilon, \quad p = (\gamma - 1) \rho \varepsilon.
\end{aligned}$$

The set of equations is supplemented by the Poisson equation for the potential of the stars and dark matter component:

$$\begin{aligned}
\frac{\partial n}{\partial t} + \nabla \cdot (n \vec{v}) &= \mathcal{D} - \mathcal{S}, \\
\frac{\partial n \vec{v}}{\partial t} + \nabla \cdot (n \vec{v} \vec{v}) &= -\nabla \Pi - n \nabla(\Phi) + \vec{u} \mathcal{D} - \vec{v} \mathcal{S}, \\
\frac{\partial \rho W}{\partial t} + \nabla \cdot (\rho W \vec{v}) &= -\nabla \cdot (\Pi \vec{v}) - (n \nabla(\Phi), \vec{v}) - \Gamma + \varepsilon \frac{\mathcal{D}}{\rho}, \\
\frac{\partial \Pi_{\xi\xi}}{\partial t} + \nabla \cdot (\Pi_{\xi\xi} \vec{v}) &= -2\Pi \nabla \cdot \vec{u} - \Gamma + \varepsilon \frac{\mathcal{D}}{3\rho}, \\
\rho W &= \frac{1}{2} \rho \vec{v}^2 + \frac{\Pi_{xx} + \Pi_{yy} + \Pi_{zz}}{2},
\end{aligned}$$

The equation for gravity is

$$\Delta\Phi = 4\pi G(\rho + n),$$

where p is the gas pressure, ρ_H is the atomic hydrogen density, ρ_{H_2} is a molecular hydrogen density, s_{H,H_2} is the formation rate of molecular hydrogen, $\rho = \rho_H + \rho_{H_2}$ is the total density, n is the density of the stars and dark matter, \vec{u} is the gas velocity vector, \vec{v} is the stars velocity vector, ρE is the total energy density of gas, ρW is the total energy density of the stars and dark matter, Φ is the gravitational potential, ε is the internal energy of gas, γ is the ratio of specific heats, $\Pi_{\xi\xi} = (\Pi_{xx}, \Pi_{yy}, \Pi_{zz})$, \mathcal{S} is the supernova ratio feedback, \mathcal{D} is the star formation ratio, Λ is the cooling function, Γ is the supernova explosion energy.

2.2. The subgrid physics model. The subgrid physics model plays the key role in the interacting galaxy problem. In our model, we use the following processes:

1. The self-consistent chemokinetic model;
2. The star formation process;
3. The supernovae feedback mechanism; and
4. The Compton cooling function.

Chemical kinetics of the process under study is based on the condition that molecular hydrogen is formed on the surface of dust grains and dissociated by the ultraviolet Lyman–Werner photons and cosmic rays. Also, we assume the mixture of dust and gas to be uniform, which is a quite natural condition. Thus, the molecular hydrogen kinetics follows the differential equation [26]:

$$\frac{dn_{H_2}}{dt} = R_{\text{gr}}(T)n_H(n_H + 2n_{H_2}) - (\xi_H + \xi_{\text{diss}}(N_{H_2}, A_V))n_{H_2},$$

where n_{H_2} and n_H are the number densities of molecular and atomic hydrogen, respectively, N_{H_2} is the molecular hydrogen column density,

$$R_{\text{gr}}(T) = 2.2 \cdot 10^{-18} S \sqrt{T} \text{ s}^{-1}$$

is the molecular hydrogen formation rate on dust grains [27], $S = 0.3$ is the efficiency of the molecular hydrogen formation on dust [28],

$$\xi_H = 6 \cdot 10^{-18} \text{ s}^{-1}$$

is the cosmic ray ionization rate [29,30], A_V is extinction [31]. The photodissociation rate $\xi_{\text{diss}}(N_{H_2}, A_V)$ can be written down as [32]:

$$\xi_{\text{diss}}(N_{H_2}, A_V) = \xi_{\text{diss}}(0) f_{\text{shield}}(N(H_2)) f_{\text{dust}}(A_V),$$

where

$$\xi_{\text{diss}}(0) = 3.3 \cdot 1.7 \cdot 10^{-11} \text{ s}^{-1}$$

is the unshielded photodissociation rate [33],

$$f_{\text{dust}}(A_V) = \exp(-\tau_{d,1000}(A_V))$$

is the dust absorption factor [32],

$$\tau_{d,1000}(A_V) = 3.74 A_V = 10^{-21} (N(H) + N(H_2))$$

is the optical depth due to dust grains at a wavelength $\lambda = 1000 \text{ \AA}$, $N(H)$ and $N(H_2)$ are the column densities, the function for the self-shielding factor being approximated by [32]:

$$f_{\text{shield}}(N(H_2)) = \frac{0.965}{(1 + x/b_5)^2} + \frac{0.035}{\sqrt{1 + x}} \exp(-8.5 \cdot 10^{-4} \sqrt{1 + x}),$$

where

$$x = \frac{N(H_2)}{5 \cdot 10^{10}} \text{ m}^2$$

$b_5 = b/10^7 \text{ m/s}$, and b is the Doppler broadening parameter. To carry out the precise calculations for the functions $f_{\text{shield}}(N(H_2))$ and $f_{\text{dust}}(A_V)$, we should know the columns densities $N(H)$ and $N(H_2)$, for which we need to find the ultraviolet radiation cumulative field formed by the young stars. After that, we estimate the number density of molecular hydrogen n_{H_2} and determine the effective ratio of the specific heats [8]:

$$\gamma = \frac{5.5 - 1.5n_{H_2}}{3.3 - 0.5n_{H_2}}$$

The star formation ratio. The necessary conditions of the star formation process are [34]:

$$T < 10^4 K, \quad \nabla \cdot \vec{u} < 0, \quad \rho > 1.64 \frac{M_{\odot}}{pc^{-3}}.$$

We can write the star formation ratio in following form:

$$\mathcal{D} = \frac{dn}{dt} = \mathcal{C} \frac{\rho}{\tau_{\text{dyn}}} = \mathcal{C} \rho^{3/2} \sqrt{\frac{32G}{3\pi}}$$

where $\mathcal{C} = 0.034$ is the factor of efficiency of the star formation.

The supernovae feedback mechanism. The supernovae feedback ratio can be written down in the following form [35]:

$$\mathcal{S} = \Delta^{\text{SN}} = \frac{d\rho}{dt} = \beta C \frac{n}{\tau_{\text{dyn}}} = \beta C n^{3/2} \sqrt{\frac{32G}{3\pi}},$$

where $\beta = 0.1$ is the ratio of the young stars explosion. The injection energy for the explosion star of the mass of M_{\odot} is equal to 10^{51} erg, thus the heating function of the supernovae feedback can be written in the following form:

$$\Gamma = 10^{51} \frac{M^{\text{SN}}}{M_{\odot}} \text{ erg},$$

where M^{SN} is the total mass of the explosion stars in a certain volume.

The Compton cooling. The galactic gas, that was heated in the process of collision up to the temperature $\sim 10^4$ – 10^8 K, cools in the course of time. The plasma cooling rate estimated with the temperature exceeding $\sim 10^4$, is [36]:

$$\epsilon_c \simeq 10^{-22} n^2 \text{ cm}^{-3} \text{ erg},$$

where n is the plasma density given as the number of hydrogen atoms per cubic centimeter.

3. The numerical method

An original numerical method, based on a combination of the Godunov method, the operator splitting approach and the piecewise-parabolic method on a local stencil providing a high-order accuracy, was used to numerically solve the hydrodynamics equations. A set of equations is solved in the two stages: the Eulerian, where the equations without advections terms are solved without considering the subgrid physics, and the Lagrangian, where the advective transportation takes place.

3.1. The Riemann solver at the Eulerian stage. At the Eulerian step, the 1D hydrodynamics equations (along the coordinate x) can be reduced to the following non-conservation matrix form:

$$\frac{\partial}{\partial t} \begin{pmatrix} v \\ p \end{pmatrix} + \begin{pmatrix} 0 & \rho^{-1} \\ \gamma p & 0 \end{pmatrix} \frac{\partial}{\partial x} \begin{pmatrix} v \\ p \end{pmatrix} = 0.$$

We can solve the Riemann problem for this system using a Godunov-type method as described below. Let us rewrite this system in the following form:

$$\frac{\partial u}{\partial t} + B \frac{\partial u}{\partial x} = 0,$$

where

$$u = \begin{pmatrix} v \\ p \end{pmatrix}, \quad B = \begin{pmatrix} 0 & \rho^{-1} \\ \gamma p & 0 \end{pmatrix}.$$

This system is hyperbolic, and hence the matrix B can be represented as $B = R\Lambda L$, where R and L are the right-hand side and the left-hand side eigenvector matrices, respectively, and Λ is a diagonal matrix of the eigenvalues of the matrix B :

$$R = \begin{pmatrix} \frac{1}{\sqrt{1 + \gamma p \rho}} & \frac{1}{\sqrt{1 + \gamma p \rho}} \\ \frac{\rho \sqrt{\gamma p / \rho}}{\sqrt{1 + \gamma p \rho}} & -\frac{\rho \sqrt{\gamma p / \rho}}{\sqrt{1 + \gamma p \rho}} \end{pmatrix}, \quad \Lambda = \begin{pmatrix} \sqrt{\gamma p / \rho} & 0 \\ 0 & -\sqrt{\gamma p / \rho} \end{pmatrix},$$

$$L = \begin{pmatrix} \frac{\rho(\rho^{-1} + \gamma p)}{2\sqrt{1 + \gamma p \rho}} & \frac{(\rho^{-1} + \gamma p)}{2\sqrt{1 + \gamma p \rho} \sqrt{\gamma p / \rho}} \\ \frac{\rho(\rho^{-1} + \gamma p)}{2\sqrt{1 + \gamma p \rho}} & -\frac{(\rho^{-1} + \gamma p)}{2\sqrt{1 + \gamma p \rho} \sqrt{\gamma p / \rho}} \end{pmatrix},$$

Let us multiply the system with the matrix L :

$$L \frac{\partial u}{\partial t} + LR\Lambda L \frac{\partial u}{\partial x} = 0.$$

Using the identity $LR = RL = I$, where I is the unit matrix, and making the substitution $w = Lu$, the latter system can be written down as

$$\frac{\partial w}{\partial t} + \Lambda \frac{\partial w}{\partial x} = 0,$$

where Λ is a diagonal sign-definite matrix with eigenvalues

$$\lambda_1 = \sqrt{\gamma p / \rho}, \quad \lambda_2 = -\sqrt{\gamma p / \rho}.$$

To formulate the Riemann problem, we must define the values of w on the left and on the right cell interfaces. In the case of piecewise-constant functions, the initial conditions for the Riemann problem can be written as:

$$w(x, 0) = w^0(x) = \begin{cases} w^L, & x < 0 \\ w^R, & x > 0 \end{cases} = \begin{cases} Lu^L, & x < 0, \\ Lu^R, & x > 0, \end{cases}$$

where u^L and u^R are the l.h.s. and r.h.s. of the cell interface and $w^L = Lu^L$ and $w^R = Lu^R$. The latter has the analytical solution

$$w_j(x, t) = w_j^0(x - \lambda_j t).$$

We make the inverse substitution, and the solution to the Riemann problem for u will be written as $u(x, t) = Rw(x, t)$.

Now, we proceed with defining the space-averaging of the matrix B at the cell interfaces. To do this, we will use a modification of the Roe approach [37], and the average density and pressure on the cell interfaces can be written as

$$\rho = \frac{\rho_L^{3/2} + \rho_R^{3/2}}{\sqrt{\rho_L} + \sqrt{\rho_R}}, \quad p = \frac{p_L\sqrt{\rho_L} + p_R\sqrt{\rho_R}}{\sqrt{\rho_L} + \sqrt{\rho_R}}.$$

These values are used for computing the matrix B . The reason for this modification of the Roe approach is that it allows an accurate calculation of the boundary between gas and vacuum.

Finally, the solution of the normal velocity and pressure at the cell interfaces for the gas dynamic equation with the effective specific heats ratio can be written in the following form:

$$\begin{aligned} U &= \frac{u_L(-\lambda t) + u_R(\lambda t)}{2} + \\ &\quad \frac{p_L(-\lambda t) - p_R(\lambda t)}{2} \sqrt{\frac{(\sqrt{\rho_L} + \sqrt{\rho_R})^2}{\frac{\gamma_L + \gamma_R}{2}(\rho_L^{3/2} + \rho_R^{3/2})(p_L\sqrt{\rho_L} + p_R\sqrt{\rho_R})}}, \\ P &= \frac{p_L(-\lambda t) + p_R(\lambda t)}{2} + \\ &\quad \frac{u_L(-\lambda t) - u_R(\lambda t)}{2} \sqrt{\frac{\frac{\gamma_L + \gamma_R}{2}(\rho_L^{3/2} + \rho_R^{3/2})(p_L\sqrt{\rho_L} + p_R\sqrt{\rho_R})}{(\sqrt{\rho_L} + \sqrt{\rho_R})^2}}, \end{aligned}$$

the solution to the "collisionless" hydrodynamic equation takes the following form:

$$\begin{aligned} V &= \frac{v_L(-\mu t) + v_R(\mu t)}{2} + \\ &\quad \frac{\Pi_L(-\mu t) - \Pi_R(\mu t)}{2} \sqrt{\frac{(\sqrt{n_L} + \sqrt{n_R})^2}{3(n_L^{3/2} + n_R^{3/2})(\Pi_L\sqrt{n_L} + \Pi_R\sqrt{n_R})}}, \\ \Pi &= \frac{\Pi_L(-\mu t) + \Pi_R(\mu t)}{2} + \\ &\quad \frac{v_L(-\mu t) - v_R(\mu t)}{2} \sqrt{\frac{3(n_L^{3/2} + n_R^{3/2})(\Pi_L\sqrt{n_L} + \Pi_R\sqrt{n_R})}{(\sqrt{n_L} + \sqrt{n_R})^2}}, \end{aligned}$$

where

$$\begin{aligned} \lambda &= \sqrt{\frac{\frac{\gamma_L + \gamma_R}{2}(p_L\sqrt{\rho_L} + p_R\sqrt{\rho_R})}{\rho_L^{3/2} + \rho_R^{3/2}}}, \quad \mu = \sqrt{\frac{3(\Pi_L\sqrt{n_L} + \Pi_R\sqrt{n_R})}{n_L^{3/2} + n_R^{3/2}}}, \\ q_L(-\nu t) &= q_i^R - \frac{\nu t}{2h} \left(\Lambda q_i - q_i^6 \left(1 - \frac{2\nu t}{3h} \right) \right), \\ q_R(\nu t) &= q_i^L + \frac{\nu t}{2h} \left(\Lambda q_i + q_i^6 \left(1 - \frac{2\nu t}{3h} \right) \right). \end{aligned}$$

Building a parabola and defining the parameters q_i^R , q_i^L , Λq_i , q_i^6 are discussed in the next subsection.

3.2. The construction of a piecewise-parabolic function. We will construct a piecewise-parabolic function $q(x)$ at segments $[x_{i-1/2}, x_{i+1/2}]$ of a regular mesh with a step h . The general form of a local parabola [22] is

$$q(x) = q_i^L + \xi(\Lambda q_i + q_i^{(6)}(1 - \xi)),$$

where q_i is a value at the center of a cell satisfying the equation

$$q_i = \frac{1}{h} \int_{x_{i-1/2}}^{x_{i+1/2}} q(x) dx,$$

$\xi = (x - x_{i-1/2})h^{-1}$, $\Lambda q_i = q_i^L - q_i^R$, and $q_i^{(6)} = 6(q_i - (q_i^L + q_i^R)/2)$. For constructing the values $q_i^R = q_{i+1}^L = q_{i+1/2}$, the interpolation function of fourth order was used:

$$q_{i+1/2} = \frac{q_i + q_{i+1}}{2} - \frac{\delta q_{i+1} - \delta q_i}{6}.$$

where $\delta q_i = (q_{i+1} - q_{i-1})/2$.

Below we present an algorithm for constructing the local parabola. The input for this algorithm are values q_i at the center of cells. The output of the algorithm are local parabolas at segments $[x_{i-1/2}, x_{i+1/2}]$.

Step 1. We construct $\delta q_i = (q_{i+1} - q_{i-1})/2$. For this procedure we use values q_{i+1} and q_{i-1} on the neighboring cells. Due to the lack of extrema on the parabola, we must modify the formula for δq_i :

$$\tilde{\delta} q_i = \begin{cases} \min(|\delta q_i|, 2|q_{i+1} - q_i|, 2|q_i - q_{i-1}|) \operatorname{sgn}(\delta q_i), & (q_{i+1} - q_i)(q_i - q_{i-1}) > 0, \\ 0, & (q_{i+1} - q_i)(q_i - q_{i-1}) \leq 0. \end{cases}$$

In the case a parallel implementation of this procedure by means of the MPI library, we must exchange an outside layer. After that, we can compute values on the boundary:

$$q_i^R = q_{i+1}^L = q_{i+1/2} = \frac{q_i + q_{i+1}}{2} - \frac{\tilde{\delta} q_{i+1} - \tilde{\delta} q_i}{6}.$$

Step 2. We can construct a parabola at a local segment by the formulas:

$$\Lambda q_i = q_i^L - q_i^R, \quad q_i^{(6)} = 6(q_i - (q_i^L + q_i^R)/2).$$

In the case of non-monotonicity of a local parabola, we must correct boundary values q_i^L and q_i^R by the formulas

$$\begin{aligned}
q_i^L = q_i^R = q_i & \quad \text{if } (q_i^L - q_i)(q_i - q_i^R) \leq 0, \\
q_i^L = 3q_i - 2q_i^R & \quad \text{if } \Lambda q_i q_i^{(6)} > (\Lambda q_i)^2, \\
q_i^R = 3q_i - 2q_i^L & \quad \text{if } \Lambda q_i q_i^{(6)} < -(\Lambda q_i)^2.
\end{aligned}$$

These parabolas may have a discontinuity on the boundary of a cell. In this case, we solve the Riemann problem. In the classical piecewise-parabolic method, parabolas are continuous and this is an important feature of the PPML approach.

For constructing the Riemann solver, we must use the integral by means of the Riemann characteristic $\pm\lambda t$ on the left and on the right from the cell interface, and these values can be written in the following form:

$$\begin{aligned}
q_L(-\lambda t) &= \frac{1}{\lambda t} \int_{x_{i+1/2}-\lambda t}^{x_{i+1/2}} q(x) dx = q_i^R - \frac{\lambda t}{2h} \left(\Lambda q_i - q_i^{(6)} \left(1 - \frac{2\lambda t}{3h} \right) \right), \\
q_R(\lambda t) &= \frac{1}{\lambda t} \int_{x_{i+1/2}}^{x_{i+1/2}+\lambda t} q(x) dx = q_i^L + \frac{\lambda t}{2h} \left(\Lambda q_i + q_i^{(6)} \left(1 - \frac{2\lambda t}{3h} \right) \right).
\end{aligned}$$

3.3. The Riemann solver at the Lagrangian stage. This system can be presented in the following general form:

$$\frac{\partial f}{\partial t} + \nabla \cdot (f\vec{v}) = 0,$$

where f can be the density ρ , the momentum density $\rho\vec{v}$, the total energy density E , or the internal energy density ϵ . The Lagrangian step describes the advective transport of all hydrodynamics variables. To solve the system of equations, we use a Godunov-type method. For the calculation of the fluxes $F = f\vec{v}$ at the cell interfaces we use a 1D linearized analogue of the system

$$\frac{\partial f}{\partial t} + v_x \frac{\partial f}{\partial x} = 0.$$

This system has a trivial eigenvalue decomposition: the eigenvalue is equal to v_x and the module of the eigenvalue is $\lambda = |v_x|$. In this case, the eigenvalue is not a sign-definite variable, and therefore the solution can be written in the following form:

$$F = \begin{cases} v_x f_L(-\lambda t), & v_x \geq 0, \\ v_x f_R(\lambda t), & v_x < 0, \end{cases}$$

where $f_L(-\lambda t)$ and $f_R(\lambda t)$ are piecewise-parabolic functions and the velocity at the cell interfaces can be written in the form

$$v_x = \frac{v_L \sqrt{\rho_L} + v_R \sqrt{\rho_R}}{\sqrt{\rho_L} + \sqrt{\rho_R}}.$$

The numerical scheme for a 1D system can be written as

$$\frac{f_i^{n+1} - f_i^{n+1/2}}{\tau} = -\frac{F_{i+1/2} - F_{i-1/2}}{h}.$$

The "Big" values with a half-integer index are a flux on a corresponding cell, and the values with an integer index are hydrodynamic variables. For computing f -flux, the PPML approach is used.

3.4. The dual energy formalism. After solving the gravitational gas dynamics equations, the original procedure is performed for the adjustment in order to save the total energy of the system. The re-normalization is of the velocity vector length, its direction remaining the same (on the gas-vacuum boundary) by means of the formula

$$|\vec{v}| = \sqrt{2(E - \epsilon)} \quad \text{if } \frac{E - \vec{v}^2/2}{E} \geq 10^{-3}.$$

The entropy (or the internal energy) correction [38] is done by the formula

$$|\rho\epsilon| = \left(\rho E - \frac{\rho \vec{v}^2}{2} \right) \quad \text{if } \frac{E - \vec{v}^2/2}{E} < 10^{-3}.$$

Such a modification of the method keeps the detailed energy balance and ensures a non-decrease of the entropy.

3.5. The Poisson solver. After the gas values are computed the Poisson equation is solved for obtaining the gravitational potential. The Poisson equation is solved by the Fourier transform method. The 27-point stencil is used for the approximation of the Poisson equation:

$$f_{ikl} = \sum_{j,m,n} f_{jmn} \exp\left(i\left(\frac{\pi j}{I} + \frac{\pi km}{K} + \frac{\pi ln}{L}\right)\right).$$

It results in the following scheme for the Poisson equation in the Fourier space:

$$\Phi_{jmn} = \frac{\frac{2}{3}\pi h^2 \rho_{jmn}}{1 - \left(1 - \frac{2 \sin^2(\frac{\pi j}{I})}{3}\right) \left(1 - \frac{2 \sin^2(\frac{\pi m}{K})}{3}\right) \left(1 - \frac{2 \sin^2(\frac{\pi n}{L})}{3}\right)}.$$

Thus, the scheme consists of the following steps:

1. Transformation of the values into the harmonic space;
2. Evaluation of the potential harmonics from the density harmonics; and
3. Inverse transformation of the potential values.

The boundary conditions for the Poisson equation fully define the solution of the gravitational dynamics problem. Due to this reason, the computation of these boundary conditions is of great importance. It is known that the potential of an object could be considered to be zero if a distance from the object is infinite. The fact is that the boundary conditions must be set at a finite distance from the gas object. In the present work, the following technique for the boundary conditions is proposed: let us assume that the mass of a gas body is concentrated at the center of the computational domain, and the value of the potential is inversely proportional to the distance from the boundary with respect to the center of the domain. However, this treatment of the boundary conditions does not take changes of the gas cloud structure into account. This means that these boundary conditions will give a wrong distribution of the gravitational potential when either the size of the domain is too small or the gas is spreading in the whole domain. This incorrect representation of the potential can easily result in a perversion of the physical situation as a whole. This problem is solved with the boundary conditions evaluated via the inertia moments, using the static, axial and centrifugal inertia moments.

3.6. Parallel implementation. The numerical method was implemented as a prototype of the software system AstroPhi 2.0 in order to use the hybrid supercomputers fit into Intel Xeon Phi accelerators. This code appears to be a natural extension of the AstroPhi code [39]. For the computational experiments, an experimental node of an ultradense solution RSC PetaStream was used. The usage of only Intel Xeon Phi accelerators as computation modules makes its distinctive feature. Apparently, such an architecture appears to be the most promising as the basis for the first exaflop supercomputer. With regard to the software system construction the code is the hybrid MPI/OpenMP native implementation with a high degree of parallelism. Namely, in the case of using Intel Xeon Phi accelerators only, it is necessary to efficiently develop every program cycle per cell of the stage complexity. Otherwise, due to a lower performance of an Intel Xeon Phi core as compared to that of CPU, we arrive at the situation when one low-cost stage can stop the whole scalability. Such a situation takes place in the GPUPEGAS code [16] at the time step computation, and the problem remains unsolved for graphic accelerators, but it is solved for Intel Xeon Phi accelerators. To study the scalability on the mesh with 512^3 size we have performed a series of tests to investigate the effect of the number of accelerator cores on the code speed-up. Thus, the time for computing a single time

step using one accelerator core was 182.466 seconds, and with an increase in the number of cores up to 240 the time was 3.408 seconds, with 54 times speedup. With the use of 8 Intel Xeon Phi 7120 accelerators the scalability reached 99.87%. Comparing the time for computing a single time step using a maximum number of Intel Xeon Phi cores, which makes 3,408 seconds, with that of 12-core Intel Xeon E5-2697 processor, which makes 8.987 seconds, we attained 2.63 speed-up with the Intel Xeon Phi accelerator as compared to the 12-core processor Intel Xeon E5-2697.

4. The numerical simulation of interacting galaxies

Two galaxies are set in the self-gravitating hydrodynamic cloud and the stars/dark matter cloud with an equilibrium profile, differential rotation profile

$$v_\phi = \sqrt{r \frac{\partial \Phi}{\partial r}},$$

where r is a cylindric radius. The mass of every galaxy is equal to $M = 10^{13} M_\odot$. The clouds move in the opposite directions with the velocities

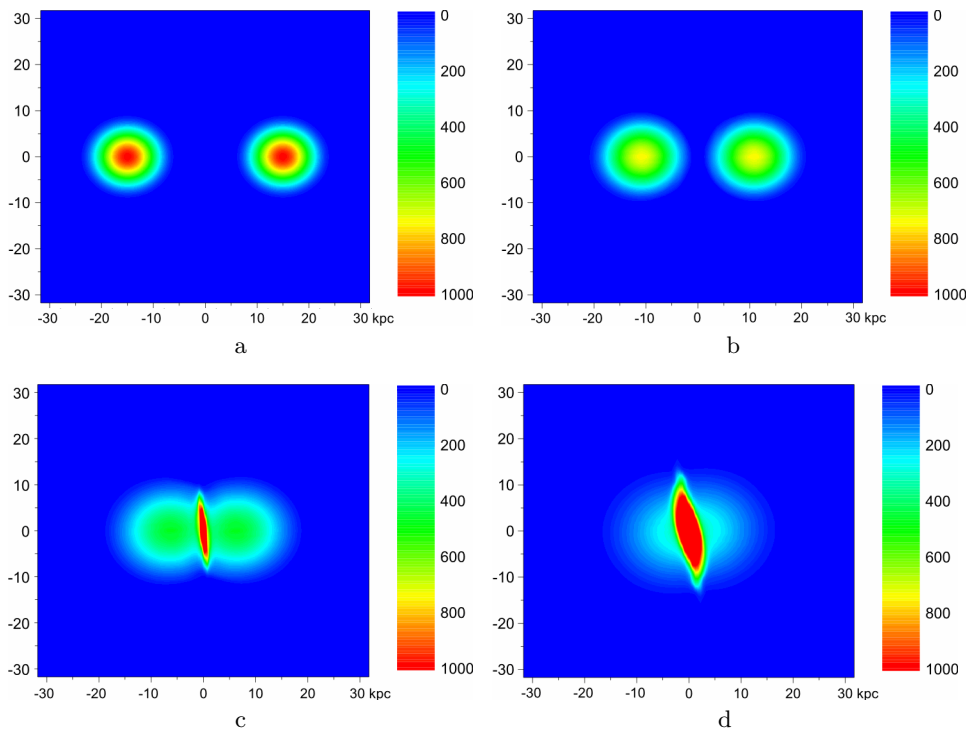


Figure 1. The column density in $M_\odot pc^{-2}$ of gas component at $t = 0$ myr (a), 40 myr (b), 80 myr (c), and 120 myr (d)

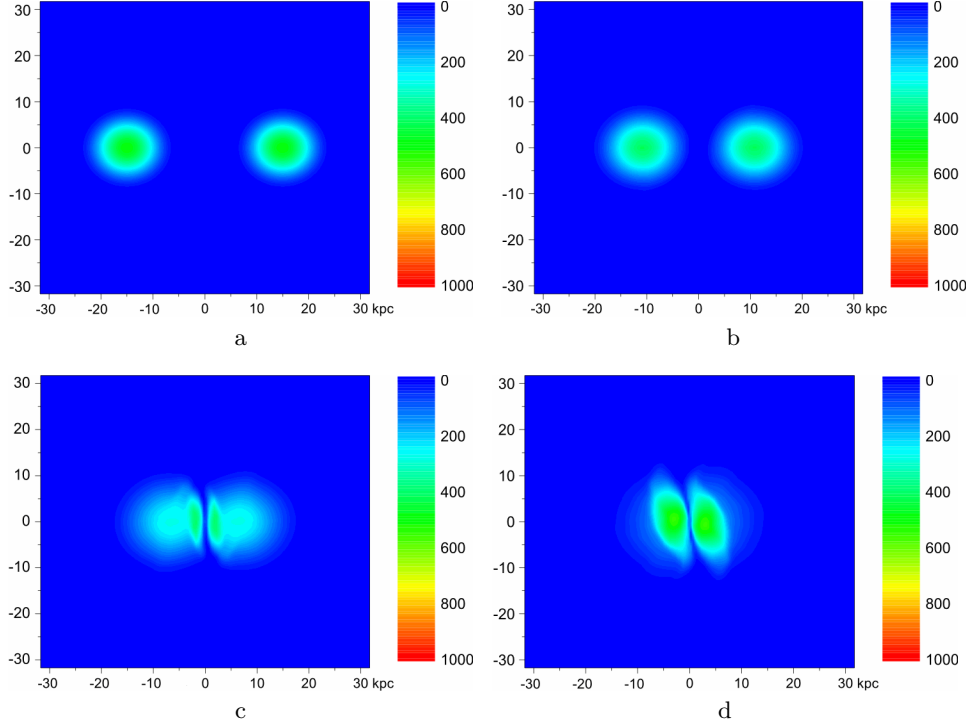


Figure 2. The column density in $M_{\odot}pc^{-2}$ of stars and dark matter component at $t = 0$ myr (a), 40 myr (b), 80 myr (c), and 120 myr (d)

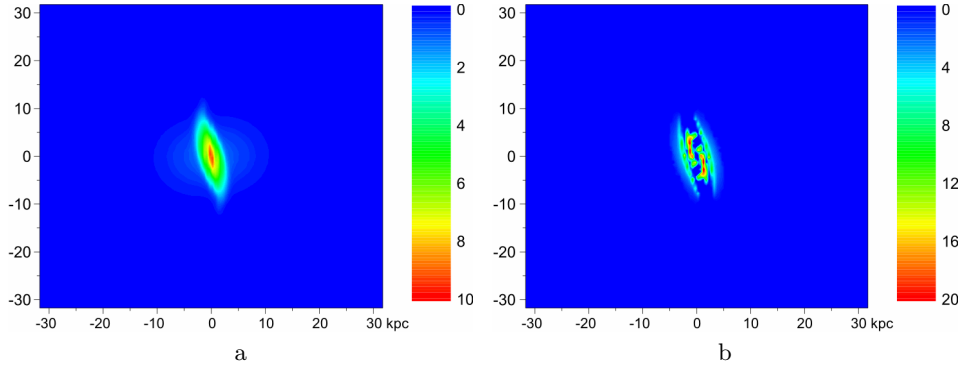


Figure 3. The column density in $M_{\odot}pc^{-2}$ of molecular hydrogen (a) and the ratio of star formation in $M_{\odot}pc^{-2} \text{ myr}^{-1}$ (b) at $t = 120$ myr

$v_{cr} = 800$ km/s. The simulation results are presented in Figures 1–3.

The pictures show one scenario of interacting galaxies, after collision of galaxies starting the process of the star formation and molecular hydrogen formation.

5. Conclusion

In this paper, an approach to constructing a low-dissipation numerical method is described. The method is based on a combination of the operator-splitting method, the Godunov method, and the piecewise-parabolic method on a local stencil. In this paper, we have presented one of the approaches to simulate the interacting galaxies problem in a minimal subgrid physics model. The model is based on the solution of the multi-component and two-phase one-velocity hydrodynamic equations with a variable specific heats ratio.

References

- [1] Tutukov A., Lazareva G., Kulikov I. Gas dynamics of a central collision of two galaxies: Merger, disruption, passage, and the formation of a new galaxy // *Astronomy Reports*. — 2011. — Vol. 55. — P. 770–783.
- [2] Schweizer F. Merger-induced starbursts // *Astrophysics and Space Science Library*. — 2005. — Vol. 329. — P. 143–152.
- [3] Sol Alonso M., Lambas D., Tissera P., Coldwell G. Active galactic nuclei and galaxy interactions // *Monthly Notices of the Royal Astronomical Society*. — 2007. — Vol. 375, Iss. 3. — P. 1017–1024.
- [4] Blecha L., Loeb A., Narayan R. Double-peaked narrow-line signatures of dual supermassive black holes in galaxy merger simulations // *Monthly Notices of the Royal Astronomical Society*. — 2013. — Vol. 429, Iss. 3. — P. 2594–2616.
- [5] Rodriguez C., Taylor G., Zavala R., et al. Hi observations of the supermassive binary black hole system in 0402+379 // *Astrophysical J.* — 2009. — Vol. 697, Iss. 1. — P. 37–44.
- [6] Combes F., Melchior A. Chemodynamical evolution of interacting galaxies // *Astrophysics and Space Science*. — 2002. — Vol. 281, Iss. 1–2. — P. 383–387.
- [7] Khopersov S., Vasiliev E., Sobolev A., Khoperskov A. The simulation of molecular clouds formation in the Milky Way // *Monthly Notices of the Royal Astronomical Society*. — 2013. — Vol. 428. — P. 2311–2320.
- [8] Glover S., Mac Low M. Simulating the formation of molecular clouds. I. Slow formation by gravitational collapse from static initial conditions // *Astrophysical J. Supplement Series*. — 2007. — Vol. 169. — P. 239–268.
- [9] Agertz O. Fundamental differences between SPH and grid methods // *Monthly Notices of the Royal Astronomical Society*. — 2007. — Vol. 380. — P. 963–978.
- [10] Tasker E., Brunino R., Mitchell N., et al. A test suite for quantitative comparison of hydrodynamic codes in astrophysics // *Monthly Notices of the Royal Astronomical Society*. — 2008. — Vol. 390. — P. 1267–1281.

- [11] Vshivkov V., Lazareva G., Snytnikov A., Kulikov I. Supercomputer simulation of an astrophysical object collapse by the fluids-in-cell method // LNCS. — 2009. — Vol. 5698. — P. 414–422.
- [12] Attwood R., Goodwin S., Whitworth A. Adaptive smoothing length in SPH // *Astronomy & Astrophysics*. — 2007. — Vol. 464. — P. 447–450.
- [13] Sijacki D., Springel V. Physical viscosity in smoothed particle hydrodynamics simulations of galaxy clusters // *Monthly Notices of the Royal Astronomical Society*. — 2006. — Vol. 371. — P. 1025–1046.
- [14] Wadsley J., Veeravalli G., Couchman H. On the treatment of entropy mixing in numerical cosmology // *Monthly Notices of the Royal Astronomical Society*. — 2008. — Vol. 387. — P. 427–438.
- [15] Mitchell N., Vorobyov E., Hensler G. Collisionless stellar hydrodynamics as an efficient alternative to N-body methods // *Monthly Notices of the Royal Astronomical Society*. — 2013. — Vol. 428. — P. 2674–2687.
- [16] Kulikov I. GPUPEGAS: a new GPU-accelerated hydrodynamic code for numerical simulations of interacting galaxies // *Astrophysical J. Supplements Series*. — 2014. — Vol. 214, Iss. 12. — P. 1–12.
- [17] Murphy J., Burrows A. BETHE-Hydro: an arbitrary Lagrangian–Eulerian multidimensional hydrodynamics code for astrophysical simulations // *Astrophysical J. Supplement Series*. — 2008. — Vol. 179. — P. 209–241.
- [18] Springel V. E pur si muove: Galilean-invariant cosmological hydrodynamical simulations on a moving mesh // *Monthly Notices of the Royal Astronomical Society*. — 2010. — Vol. 401. — P. 791–851.
- [19] Van Leer B. Towards the ultimate conservative difference scheme, V. A second order sequel to Godunov’s method // *J. Comput. Phys.* — 1979. — Vol. 32, Iss. 1. — P. 101–136.
- [20] Kurganov A., Tadmor E. New high-resolution central schemes for nonlinear conservation laws and convection-diffusion equation // *J. Comput. Phys.* — 2000. — Vol. 160. — P. 214–282.
- [21] Jin S., Xin Z. The relaxation schemes for systems of conservation laws in arbitrary space dimensions // *Communications on Pure and Appl. Math.* — 1995. — Vol. 48, Iss. 3. — P. 235–276.
- [22] Collella P., Woodward P. The Piecewise Parabolic Method (PPM) gas-dynamical simulations // *J. Comput. Phys.* — 1984. — Vol. 54. — P. 174–201.
- [23] Wattersona N.P., Deconinck H. Design principles for bounded higher-order convection schemes — a unified approach // *J. Comput. Phys.* — 2007. — Vol. 224. — P. 182–207.
- [24] Popov M., Ustyugov S. Piecewise parabolic method on local stencil for gas-dynamic simulations // *Comput. Math. and Math. Phys.* — 2007. — Vol. 47, Iss. 12. — P. 1970–1989.

-
- [25] Popov M., Ustyugov S. Piecewise parabolic method on a local stencil for ideal magnetohydrodynamics // *Comput. Math. and Math. Phys.*—2008.— Vol. 48, Iss. 3.— P. 477–499.
- [26] Bergin E., Hartmann L., Raymond J., Ballesteros-Paredes J. Molecular cloud formation behind shock waves // *Astrophysical J.*—2004.— Vol. 612.— P. 921–939.
- [27] Tielens A., Hollenbach D. Photodissociation regions. I— Basic model. II— A model for the Orion photodissociation region // *Astrophysical J.*—1985.— Vol. 291.— P. 722–754.
- [28] Cazaux S., Tielens A. H_2 Formation on grain surfaces // *Astrophysical J.*—2004.— Vol. 604.— P. 222–237.
- [29] Caselli P., Walmsley C., Terzieva R., Herbst E. The ionization fraction in dense cloud cores // *Astrophysical J.*—1998.— Vol. 499.— P. 234–249.
- [30] Bergin E., Plume R., Williams J., Myers P. The ionization fraction in dense molecular gas. II. Massive cores // *Astrophysical J.*—1999.— Vol. 512.— P. 724–739.
- [31] Van Der Tak F., Van Dishoeck E. Limits on the cosmic-ray ionization rate toward massive young stars // *Astronomy & Astrophysics.*—2000.— Vol. 358.— P. L79–L82.
- [32] Draine B., Bertoldi F. Structure of stationary photodissociation fronts // *Astrophysical J.*—1996.— Vol. 468.— P. 269–289.
- [33] Draine B. Photoelectric heating of interstellar gas // *Astrophysical J. Supplement Series.*—1978.— Vol. 36.— P. 595–619.
- [34] Katz N., Weinberg D., Hernquist L. Cosmological simulations with TreeSPH // *Astrophysical J. Supplement Series.*—1996.— Vol. 105.— P. 19–35.
- [35] Springel V., Hernquist L. Cosmological smoothed particle hydrodynamics simulations: a hybrid multiphase model for star formation // *Monthly Notices of the Royal Astronomical Society.*—2003.— Vol. 339, Iss. 2.— P. 289–311.
- [36] Sutherland R., Dopita M. Cooling functions for low-density astrophysical plasmas // *Astrophysical J. Supplement Series.*—1993.— Vol. 88.— P. 253–327.
- [37] Roe P. Approximate Riemann solvers, parameter vectors, and difference solvers // *J. Comput. Phys.*—1997.— Vol. 135.— P. 250–258.
- [38] Godunov S., Kulikov I. Computation of discontinuous solutions of fluid dynamics equations with entropy nondecrease guarantee // *Comput. Math. and Math. Phys.*—2014.— Vol. 54, Iss. 6.— P. 1012–1024.
- [39] Kulikov I., Chernykh I., Snytnikov A., et al. AstroPhi: A code for complex simulation of dynamics of astrophysical objects using hybrid supercomputers // *Computer Physics Communications.*—2015.— Vol. 186.— P. 71–80.

